Soft Matter

PAPER

View Article Online
View Journal

Cite this: DOI: 10.1039/c4sm01742k

Toward understanding the structural heterogeneity and ion pair stability in dicationic ionic liquids†

Song Li,[a] José Leobardo Bañuelos,*[bc] Pengfei Zhang,[c] Guang Feng,*[d] Sheng Dai,[ce] Gernot Rother[c] and Peter T. Cummings[a]

Received 6th August 2014
Accepted 23rd September 2014

DOI: 10.1039/c4sm01742k

www.rsc.org/softmatter

The structural and dynamical properties of dicationic ionic liquids (DILs) $[C_n(mim)_2](Tf_2N)_2$, that is, 3-methylimidazolium dications separated by an alkyl chain and with bis(trifluoromethylsulfonyl)amide as the anion, were investigated by molecular dynamics (MD) simulation in combination with small/wide-angle X-ray scattering (SWAXS) measurements. Enhanced spatial heterogeneity is observed as the DIL chain length is increased, characterized by the changes in the scattering and the increased heterogeneity order parameter (HOP). Temperature variation imposes only slight influences on the local structures of DILs compared to monocationic ionic liquids (MILs). The peaks at 0.9 $Å^{-1}$ and 1.4 $Å^{-1}$ of the structure function shift towards low Q as the temperature increases, in a similar manner to MILs, and changes in peak positions in response to temperature changes are reflected in HOP variations. However, the prepeak shift with increasing temperature is ~3 times smaller in DILs compared to MILs, and both MD and SWAXS indicate a DIL-specific prepeak shifting. Furthermore, the high ion pair/ion cage stability in DILs is indicative of high thermal stability and relative insensitivity of structural heterogeneity to temperature variation, which might be caused by the stronger Coulombic interactions in DILs.

Introduction

Spatial heterogeneity in solvent-free room temperature ionic liquids (RTILs) has been extensively investigated over the past two decades. Molecular dynamics (MD) simulation[1–3] and small-angle X-ray scattering (SAXS) studies[4–7] have revealed enhanced spatial heterogeneity in the presence of long alkyl chains of cations in RTILs. Previous studies[4,5,8] have observed that prolongation of the alkyl chain length or increased aggregation of alkyl chains corresponds to an increased intensity of a prepeak at ~0.3 $Å^{-1}$ in the structure function of RTILs obtained from either MD or SAXS. Hettige *et al.*[9] reported that the prepeak in the structure function is mostly contributed by long-range anion–anion correlations, due to their large molecular form factor. Therefore, the X-ray structure functions of RTILs are dominated by anions instead of cations. It was further demonstrated that the spatial distribution of charge and polarity alternation are directly related to the cation head–anion partial structure functions.[10] Moreover, the influence of temperature on the structural organization of long-chain RTILs has been investigated both theoretically and experimentally.[5,11,12] Shifts of the peaks in the low-Q region ($Q \leq 2.0$ $Å^{-1}$) as a function of temperature have been found. Our former study[13] on RTILs $[C_nMPy][Tf_2N]$ (n = 3, 6, 8, and 10) reveals that the prepeak located at approximately 0.3 $Å^{-1}$ shifts towards the high-Q region with an increased temperature, indicating the reduced polarity alternation distance. In contrast, the peaks at 0.9 and 1.4 $Å^{-1}$, corresponding to cation–cation/anion–anion and cation–anion correlations, respectively, are observed to shift towards low-Q regions with the increase of temperature, which is correlated with the increased distance between ions because of decreased density at high temperature as stated in the work of Santos *et al.*[5] However, Kashyap *et al.* reported that all the three peaks shift towards low Q with an increase in temperature for the RTIL tetradecyltrihexylphosphonium bis(trifluoromethyl-sulfonyl)amide ($[P_{14,666}][Tf_2N]$),[11] implicating that the temperature-dependent peak shift probably relies on the type of ionic liquids.

Recently, dicationic ionic liquids (DILs) have been receiving rapidly increasing interest due to their more concentrated charges and high electrochemical stabilities. Similar to MILs, DILs can be utilized as solvents,[14] catalysts,[15] lubricants[16] and

[a]Department of Chemical and Biomolecular Engineering, Vanderbilt University, Nashville, TN 37235, USA
[b]ISIS Facility, STFC Rutherford Appleton Laboratory, Harwell, Didcot, Oxford, OX11 0QX, UK. E-mail: jose.banuelos@stfc.ac.uk
[c]Chemical Sciences Division, Oak Ridge National Laboratory, Oak Ridge, TN 37831, USA
[d]State Key Laboratory of Coal Combustion, School of Energy and Power Engineering, Huazhong University of Science and Technology, Wuhan 430074, China. E-mail: gfeng@hust.edu.cn
[e]Department of Chemistry, University of Tennessee, Knoxville, TN 37996, USA

† Electronic supplementary information (ESI) available: Total static structure functions from MD and SWAXS, the snapshot of $[C_{12}(mim)_2](Tf_2N)_2$ at 280–360 K, the peak (Q_1, Q_2, Q_3) width as a function of temperature, radial distribution function and dication linking chain angle distribution. See DOI: 10.1039/c4sm01742k

electrolytes.[17] The performance of DIL electrolytes in supercapacitors has been reported in our recent study,[18] where we found a distinctive electrical double layer formed by DILs at the electrode surface in contrast to MILs. These different behaviors were attributed to electrostatic effects, *i.e.*, the more concentrated charge densities in DILs. It was also observed that Tf_2N-containing DILs exhibit higher capacitance than their monocationic counterparts. Moreover, the linkage alkyl chain in DILs $[C_n(mim)_2](X)_2$ ($n = 3$, 6, 9, 12; X = BF_4^-, PF_6^- and Br^-) exhibits less spatial heterogeneity in comparison with the free alkyl chain in MILs, as indicated by the lower prepeak intensity and smaller heterogeneity order parameters (HOPs) in DILs obtained from MD simulation.[19] In addition, the structure functions of MILs and DILs also exhibit sensitivity to the type of anion. However, experimental verification of the above-mentioned predictions is still missing. Currently, the high melting points (~400 K) of $[C_n(mim)_2](X)_2$ restrict their applications in the liquid phase at room temperature, whereas this is not the concern for Tf_2N-containing DILs $[C_n(mim)_2](Tf_2N)_2$ due to their lower melting point (<280 K). Therefore, there is great interest and special significance in studying the nanostructural and physicochemical properties of $[C_n(mim)_2](Tf_2N)_2$ ($n = 3$, 6, 12) at different temperatures.

To the best of our knowledge, the influence of temperature variation on the nanostructure of $[C_n(mim)_2](Tf_2N)_2$ DILs has not been previously reported, and it is still unknown whether the low-Q peaks in the structure functions of DILs show similar shifts with temperature as those of MILs. Thus, in this work, small/wide-angle X-ray scattering (SWAXS) measurements were carried out to investigate the spatial heterogeneity in dicationic $[C_n(mim)_2](Tf_2N)_2$ over a wide temperature range. MD simulations aid in the analysis and interpretation of the structural ordering at the molecular level. Furthermore, the ion pair/ion cage stability of $[C_n(mim)_2](Tf_2N)_2$ is explored using MD, and compared to monocationic $[C_n mim][Tf_2N]$ with the goal of obtaining a comprehensive interpretation of the relationship between the structural organization and dynamical properties in DILs.

Materials and methodology

Chemicals and synthesis of dicationic ionic liquids $[C_n(mim)_2](Tf_2N)_2$

Chemicals. All the chemicals, including 1,3-dibromopropane (99%); 1,6-dibromohexane (96%); 1,12-dibromododecane (98%) and 1-methylimidazole (97%), were purchased from Sigma-Aldrich Chemicals in USA and used without further treatment.

$[C_n(mim)_2](Tf_2N)_2$ ($n = 3$, 6, and 12) was prepared through the intermediate $[C_n(mim)_2](Br)_2$. Initially, 0.098 mol of dibromoalkane ($n = 3$: 1,3-dibromopropane, $n = 6$: 1,6-dibromohexane, $n = 12$: 1,12-dibromododecane) was added into 15.6 mL (0.196 mol) of 1-methylimidazole with 20 mL CH_3CN solvent drop by drop under Ar flow at room temperature. The reaction was then heated to 60 °C for 8 h in an Ar atmosphere and the organic solvent was subsequently removed under reduced pressure, yielding crude $[C_n(mim)_2](Br)_2$. The bromide salt was dissolved in 100 mL water and extracted with three 25 mL aliquots of ethyl acetate. Water was removed under vacuum heating and the remaining $[C_n(mim)_2](Br)_2$ was ion exchanged with $LiTf_2N$ in water to yield $[C_n(mim)_2](Tf_2N)_2$. The resulting product was then dissolved in 200 mL EtOAc and further purified using activated carbon (5 g, BET surface area: 1100 $m^2\ g^{-1}$). The $[C_n(mim)_2](Tf_2N)_2$ was separated by filtration and then freeze-dried for three days. The water contents of the dried ILs were estimated to be less than 0.1 wt% by Karl Fischer titration, whose influence is negligible.

Small angle X-ray scattering experiment

Small/wide-angle X-ray scattering measurements on $[C_n(mim)_2](Tf_2N)_2$ with $n = 3$, 6, and 12 were performed using the Anton Paar SAXSess mc^2 instrument at the Center for Nanophase Materials Sciences at Oak Ridge National Laboratory. The coherent scattering intensity, $I_{coh}(q)$ was collected as a function of the momentum transfer, $Q = 4\pi \sin\theta/\lambda$ where λ is the wavelength and 2θ is the scattering angle. Measurements were performed over a Q-range from 0.05–2.7 $Å^{-1}$. The samples were contained in polyimide tubes with a 1.45 mm inner diameter and 0.06 mm wall thickness. The tubes were mounted onto a stainless steel holder and sealed using HPLC fittings. The temperature was controlled using an Anton Paar TCS 120 unit capable of maintaining the temperature within ±0.1 °C. The temperature at the sample position was calibrated with respect to the temperature of the controller for this sample geometry. Measurements were conducted in the temperature range of 248 K to 380 K at approximately 20 K intervals. Scattering measurements were conducted at 40 kV and 50 mA using a 1.6 cm slit-collimated beam tuned to the Cu K_α wavelength and data were collected using an image plate detector. Transmission coefficients were obtained from measurements of the sample-attenuated direct beam intensity at 11 kV and 8 mA collected on the instrument's CCD detector. Raw scattering data corrections included normalization to the incident beam intensity and sample attenuation, and background scattering subtraction. Water scattering was used to calibrate all scattering intensities to absolute units of differential scattering cross section per unit volume, $I(Q) = (1/V)d\Sigma/d\Omega$ (cm^{-1}).

The structure functions, $S(Q)$, were computed by using the program PDFgetX2 (ref. 20) and the data was corrected according to:

$$S(Q) = \frac{\left(I(Q) - \sum_i \chi_i f_i^2\right)}{\left(\sum_i \chi_i f_i\right)^2}$$

Here, χ_i and f_i are the atomic concentration and the form factor of atomic species i, respectively. Additionally, the data were corrected for sample self-absorption, multiple scattering, and Compton scattering. The room-temperature $S(Q)$ data for the series are displayed in Fig. 2. The position, amplitude and width of the peaks of the scattering curves were fit in the range of Q from 0.08 to 1.9 $Å^{-1}$ with Gaussian curves. Three Gaussian

curves ($N = 3$) were used to fit the $n = 12$ DIL data, and two ($N = 2$) were used to fit the $n = 6$ and $n = 3$ DIL data.

Molecular dynamics (MD) simulation

The force field used for dications of $[C_n(mim)_2](Tf_2N)_2$ ($n = 3$, 6, and 12) was adapted from the all-atom force field developed by Yeganegi *et al.*,[21] which has been validated by reproducing the experimental densities of DILs with high accuracy.[22] The force field parameters for anions and monocationic $[C_n mim][Tf_2N]$ ($n = 3$ and 6) were taken from the study of Lopes' group.[23] All hydrogen bonds were constrained during the simulation using the LINCS algorithm[24] and a 1.1 nm-cutoff was used for van der Waals interactions. Long-range electrostatic interactions were evaluated using the particle mesh Ewald (PME) method.[25] Periodic boundary conditions (PBCs) were applied in three dimensions. All simulations were performed using the MD package Gromacs.[26] A simulation box consisting of ~1000 ion pairs at low density was initialized at 800 K for 1 ns, followed by a 6 ns equilibration at 280, 320 and 360 K in the isobaric–isothermal ensemble. The equilibrated box size is in the 8–10 nm range, which is sufficiently large to accurately represent the low-Q peaks above 0.15 $Å^{-1}$ in the structure function. Trajectories from a 2 ns production run generated at 1 bar and target temperatures were used for further analysis. Total static structure factors were calculated using the following equation,[27]

$$S(Q) = \frac{\sum_{\alpha\beta} \chi_\alpha \chi_\beta f_\alpha(\mathbf{Q}) f_\beta(\mathbf{Q}) 4\pi\rho \int_0^{r_c} [g_{\alpha\beta}(r) - 1] r^2 \frac{\sin(\mathbf{Q}r)}{\mathbf{Q}r} \mathrm{d}r}{\left[\sum_{\alpha\beta} \chi_\alpha f_\alpha(\mathbf{Q})\right]^2}$$

where χ_α and χ_β are the mole fractions of atom of species α and β, respectively. Q is the wave vector, $f_\alpha(Q)$ is the form factor of atom species α, and $g_{\alpha\beta}(r)$ is the correlation function of atom species α and β, and r_c is the integration cutoff, which equals one half of the simulation box. The heterogeneity order parameter (HOP) is used to quantify the effect of increasing the alkyl chain on the spatial heterogeneity of DILs and MILs, and is calculated from[2,28]

$$h = \frac{1}{N_s} \sum_{i=1}^{N_s} \sum_{j=1}^{N_s} \exp\left(\frac{-r_{ij}^2}{2\sigma^2}\right)$$

where N_s is the total number of sites in the system, r_{ij} is the distance between sites i and j corrected by periodic boundary conditions, and $\sigma = \frac{L}{N_s^{1/3}}$ with L, the length of the cubic simulation box.

The value of h increases with increasing spatial heterogeneity because a tighter packing of sites results in a smaller r_{ij}, which leads to a larger h.

Results and discussion

Structural heterogeneity in $[C_n(mim)_2](Tf_2N)_2$

The impact of long alkyl chains in BF_4-containing DILs on aggregation has been reported in a previous MD study.[19] In our work on $[C_n(mim)_2](Tf_2N)_2$, a similar self-aggregation behavior was found, as visualized in the MD snapshots shown in Fig. 1.

Fig. 1 shows that the nonpolar alkyl chains segregate from the polar cation heads and anions in the long-chain $[C_n(mim)_2](Tf_2N)_2$. This phenomenon is more pronounced for longer alkyl chains and reflected in the HOP values shown in Table 1. According to the study of Wang *et al.*, the HOP value for homogenously distributed ideal particles is ~15.74, and the heterogeneous system exhibits an HOP above 15.74.[2] All HOPs presented in Table 1 are slightly higher than 15.74, indicating a heterogeneous distribution of cation heads, anions and chains. The HOP is increased as the linking alkyl chain length is increased, although the increase is not as significant as what is observed in MILs in our previous work.[19] On average, the cation chain exhibits higher HOP values than both cation heads and anions, which can be attributed to the stronger hydrophobic interaction between alkyl chains. Recently, Shimizu *et al.* revealed the relationship between the size/shape of nonpolar aggregates and the alkyl chain length by introducing statistical functions,[29] in which the size of nonpolar aggregates increases with the alkyl chain and a transition from the prolate to oblate aggregate with increased alkyl chain. Such tendency in DILs should not be as evident as in MILs because of the insignificant aggregation phenomenon in DILs, which will be verified in the future work. This method was then adopted in the study of Bernardes *et al.* on ionic liquids with single and double long alkyl side chains.[30] Different from DILs, monocationic ILs with double long alkyl side chains exhibit greatly enhanced heterogeneity in contrast to those with a single free alkyl chain.

The total static structure functions of $[C_n(mim)_2](Tf_2N)_2$ were calculated from MD simulations and compared with the experimental data measured by SWAXS. Fig. 2 shows the modelled (b) and experimental (c) $S(Q)$ at 320 K.

Though the structure functions obtained from MD and SWAXS do not exactly align, they share several important features qualitatively. Both results show the presence of a low-Q peak located at approximately 0.35–0.4 $Å^{-1}$ in the structure function of $[C_{12}(mim)_2](Tf_2N)_2$ (this feature is absent in both MD and SWAXS results for $n = 3$ and $n = 6$). This observation provides further support for the enhanced heterogeneity in long-chain DILs as demonstrated in the previous section. Both MD and SWAXS structure functions exhibit peaks located at just above 0.8 $Å^{-1}$ (Q_2) and just below 1.4 $Å^{-1}$ (Q_3). Several effects could be responsible for the difference in magnitudes of $S(Q)$ between MD and SWAXS, including inaccuracies of the force

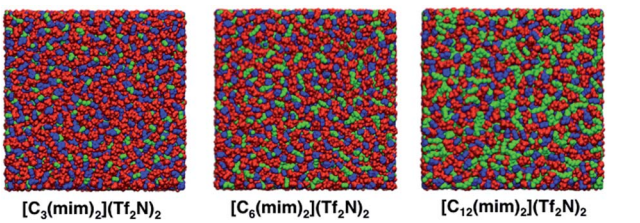

Fig. 1 Snapshots of $[C_n(mim)_2](Tf_2N)_2$ from MD simulation at 320 K: red, anion; blue, cation head; green, alkyl chain.

Table 1 Heterogeneity order parameters for head, anion and chain of $[C_n(mim)_2](Tf_2N)_2$ (n = 3, 6, and 12) at 320 K

	Head	Anion	Chain
$n = 3$	15.76 ± 0.00038	15.77 ± 0.0009	15.79 ± 0.0017
$n = 6$	15.77 ± 0.00048	15.78 ± 0.0007	15.81 ± 0.0017
$n = 12$	15.81 ± 0.00128	15.81 ± 0.0015	15.92 ± 0.0047

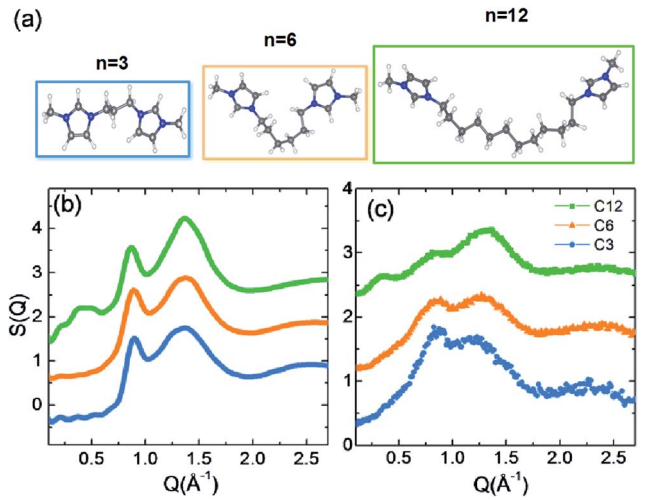

Fig. 2 Structure factors ($S(Q) - 1$) of n = 3, 6, and 12 DIL from (b) MD simulation and (c) from experiments. The curves are displayed offset for clarity and the Q starts from 0.15 Å^{-1} in Fig. 2b and c because of the limitation of periodic boundary conditions in MD simulations. The amount of scattering at Q < 0.7 Å^{-1} increases as n increases finally forming a distinct correlation Q_1 at ~0.4 Å^{-1} for n = 12. Peaks Q_1 and Q_2 are clearly discerned in the n = 12 DIL.

field used in MD, or errors in the absorption correction applied to the X-ray data. However, note that the ratio of the Q_2 to Q_3 peak intensities decreases with increasing chain length in both experiments and simulations, which increases confidence in the reliability of this novel result.

Partial structure function analysis helps to better understand these results and determines the specific contributions of local organization in DILs. Fig. 3 shows the origins of the three main peaks in the structure function from MD calculations. Q_3 is mainly due to cation–anion and cation–cation correlations based on inspection of the partial structure functions shown in Fig. 3; while anion–anion correlations make a negative contribution in this region. Anion–anion correlations make a major contribution to the peak at Q_2, which coincides with a pronounced minimum of the cation–anion structure function. In contrast to monocationic $[C_nMPy][Tf_2N]$ and BF_4-containing DILs, the prepeak position for $[C_{12}(mim)_2](Tf_2N)_2$ is found at 0.4 Å^{-1} (Q_1). This value agrees with the study of Bodo *et al.*, which found a prepeak at 0.4 Å^{-1} for $[C_{12}(mim)_2](Tf_2N)_2$ from neutron scattering and MD simulation analysis.[31] As discussed above, Q_1 originates primarily from anion–anion correlations.

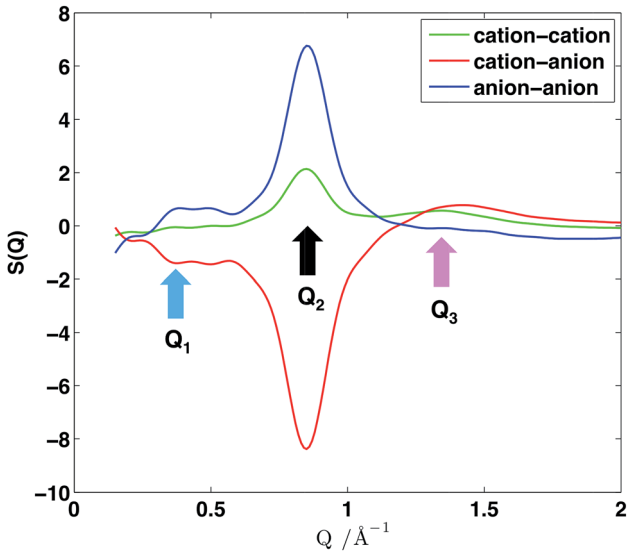

Fig. 3 Partial structure functions contributed by cation–cation, cation–anion and anion–anion correlations of $[C_{12}(mim)_2](Tf_2N)_2$ from MD simulations at 320 K.

Temperature influence

Although a large body of research focuses on the spatial heterogeneity in ionic liquids, the influence of temperature on their structural organization is rarely reported. Previous studies have investigated the physical basis of the observed temperature-dependent peak shifts in the structure functions of MILs, but not for DILs.

In both SWAXS and MD (Fig. 4), Q_2 and Q_3 slightly shift towards low Q as temperature increases. Our previous study on $[C_nMPy][Tf_2N]$ showed that the peaks at 0.9 Å^{-1} and 1.4 Å^{-1} shift to low Q with an increasing temperature, whereas the prepeak at 0.3 Å^{-1} shifted to high Q due to the decreased size of aggregates formed by alkyl chains. However, in this study on DILs, the shift of Q_1 to lower Q is trivial, as observed in MD simulation in Fig. S1 of ESI.† In SWAXS of Fig. 4, we show that the prepeak position (Q_1) in general shifts to high Q as temperature increases. However, in the temperature range of 280–360 K, Q_1 is insensitive to the variation of temperature, which is substantiated by the visual inspection of the snapshots obtained from MD simulations at different temperatures, shown in Fig. S2.† The radial distribution functions (RDFs) of cation head–head, head–anion and anion–anion of $[C_{12}(mim)_2](Tf_2N)_2$ at 280, 320 and 360 K were calculated (Fig. S3†), in which the differences of RDFs at varying temperatures are nearly invisible, consistent with the observation in the structure function.

In addition, the nearly constant heterogeneity order parameters for dicationic $[C_{12}(mim)_2](Tf_2N)_2$ calculated at different temperatures from MD simulation (Table 2) indicate that the structural heterogeneity does not significantly change in the temperature range of 280 K to 360 K. Although HOPs are not entirely constant as the temperature increases, such variation is negligible and, which does not cause evident enhancement or

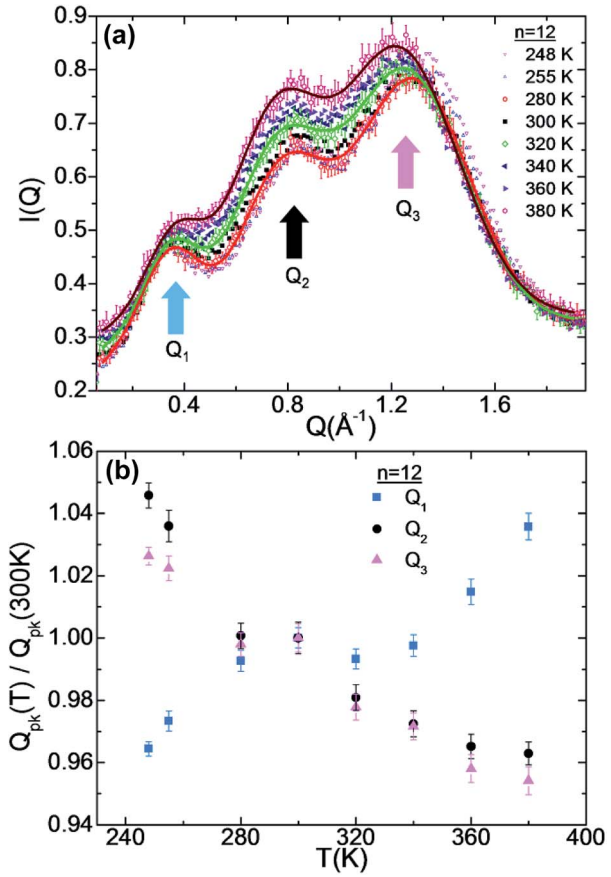

Fig. 4 (a) Scattering intensities for $n = 12$ DIL at varying temperatures; (b) variation in position of Q_1, Q_2, and Q_3 peaks for $n = 12$ DIL. Q_1(300 K) = 0.35 Å^{-1}, Q_2(300 K) = 0.776 Å^{-1}, Q_3(300 K) = 1.283 Å^{-1}, and the respective *d*-spacings according to $2/Q$ are 18.0 Å, 8.1 Å and 4.9 Å.

Table 2 Heterogeneity order parameters for head, anion and chain of $[C_{12}(mim)_2](Tf_2N)_2$ at 280 K, 320 K and 360 K

Temperature (K)	Head	Anion	Chain
280	15.80 ± 0.0009	15.81 ± 0.0014	15.91 ± 0.0031
320	15.80 ± 0.0012	15.81 ± 0.0015	15.92 ± 0.0047
360	15.80 ± 0.0014	15.81 ± 0.0019	15.90 ± 0.0048

weakening of the aggregation in long-chain DILs. Interestingly, a correlation is observed between the HOP and the peak widths in the experimental data as a function of temperature, as shown in Fig. S4.† The width of low-Q peak, Q_1, in the $n = 12$ DIL is relatively unchanged, in correspondence to the negligible HOP variation. However, the Q_3 peaks broaden toward low Q with the increase in temperature. The Q_2 peak, due primarily to anion–anion correlations, becomes sharper with increased temperature in all three studied DILs. This behavior might be caused by the interplay of weakened hydrophobic interactions and strong, temperature-independent electrostatic interactions between charge centers, leading to more well-defined ordering of ions at higher temperature.

The influence of temperature on the structural heterogeneity of DILs is compared to that of MILs, as shown in Fig. 5. It is clear that MILs exhibit the higher prepeak intensity than DILs regardless of the temperature, which is in agreement with our previous report that the free alkyl tails in MILs are able to form more significant aggregation than the linkage chains in DILs. The peak intensity at 0.9 Å^{-1} is slightly decreased for DILs. According to partial structure functions shown in Fig. 3, the peak at 0.9 Å^{-1} (Q_2) results from the positive contributions by the anion–anion/cation–cation and negative contribution by cation–anion correlations at 7 Å in real distance. This is correlated with the enhanced correlations in MIL at this distance as shown in RDFs of Fig. S5.† Although similar cation–anion and anion–anion correlation at 7 Å for DIL and MIL are observed, the cation–cation correlation (Fig. S5a†) of MIL at 7 Å is significantly higher than that of DIL. Thus, the combined effects of ion correlations result in increased Q_2 of MIL, whereas the peak intensity at 1.4 Å^{-1}, mainly contributed by the cation–cation and cation–anion correlations at 4.5 Å, is decreased. Similarly, DIL and MIL exhibit nearly identical cation–anion correlations, but DIL shows enhanced cation–cation correlation at 4.5 Å, indicating increased Q_3 of DIL. The weaker ion interactions at 7 Å and stronger correlations at 4.5 Å presented in DIL match the observations of structure functions in Fig. 5 very well.

Another phenomenon noticed is that the prepeak in monocationic $[C_6mim][Tf_2N]$ shifts towards high Q as temperature increases, similar to our previous finding in $[C_nMPy][Tf_2N]$.[13] However, it is difficult to identify a trend in the dicationic $[C_{12}(mim)_2](Tf_2N)_2$ prepeak position with increased temperature, *i.e.*, the prepeak shift is much smaller in magnitude. On this much smaller scale, the prepeak appears to move towards lower Q in simulation, but moves to higher Q in the experiment. A shift to low Q has been reported for monocationic $[P_{14,666}][Tf_2N]$ from SAXS and MD simulation.[11] We speculate that the temperature-dependent prepeak shifts are in fact dependent on the type of ionic liquids or temperature sensitivity of the aggregates formed by the long alkyl chains.

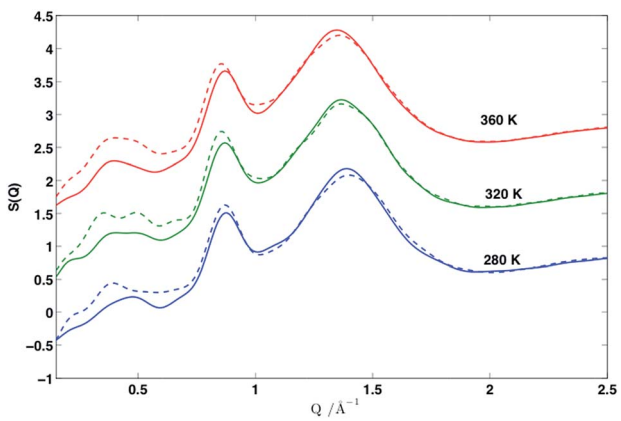

Fig. 5 Total static structure functions (with $Q > 0.15$ Å^{-1}) of dicationic $[C_{12}(mim)_2](Tf_2N)_2$ (solid lines) and monocationic $[C_6mim][Tf_2N]$ (dashed lines), calculated from MD simulations. The blue, green and red lines denote the data obtained at 280, 320 and 360 K, respectively.

To glean additional insight into the nature of these interactions, it is helpful to compare the experimentally obtained relative peak shift in the $n = 12$ DIL, shown in Fig. 4b, with the relative peak shift in the $n = 10$ MIL $[C_nMPy][Tf_2N]$, which was reported previously[13] by us over the same temperature range (~300–360 K). The shifts of the second peaks, near 0.8 $Å^{-1}$, are 2.6% and 3.5% for $[C_{10}MPy][Tf_2N]$ and $[C_{12}(mim)_2](Tf_2N)_2$ ionic liquids, respectively. This correlation is due to close-range electrostatic interactions. It seems reasonable that these changes are comparable because similar charged species are found in both RTILs. However, the shifts in the low Q peak are 4.8% for $[C_{10}MPy][Tf_2N]$ and only 1.5% for $[C_{12}(mim)_2](Tf_2N)_2$. This difference by more than a factor of 3 in the relative peak position changes indicates that, on the scale of the alkyl chain separation, the DIL structure is more stable and insensitive to temperature variation than MIL. According to our discussion above, it is noteworthy that the position of a given peak is determined by multiple correlations. Therefore, it is difficult to attribute the resulted peak to a single correlation. On the other hand, the temperature dependence of a shoulder or the neighboring peak may also result in a peak shift, which greatly increases the difficulty of exploring the origin of peak shift by temperature variations.

This prepeak shift behavior supports the results of the HOP analysis and of the ion pair stability analysis present in the next section, which point to a structurally stable DIL as temperature is varied. The small prepeak shift in the $n = 12$ DIL explains the difficulty in following this change in the MD simulation. The peaks at 0.9 $Å^{-1}$ and 1.4 $Å^{-1}$ in both $[C_6mim][Tf_2N]$ and $[C_{12}(mim)_2](Tf_2N)_2$ shift to lower Q, which indicates a decrease in density at higher temperatures, leading to greater distances between ions. However, this effect is less evident in dicationic $[C_{12}(mim)_2](Tf_2N)_2$ probably owing to its high viscosity compared to monocationic $[C_6mim][Tf_2N]$.

In Fig. 6, we present a schematic representation of how the $n = 12$ DIL structure changes with temperature, that agrees with the experimental and simulation results. Specifically, the average close-contact ion separation increases with temperature. As the temperature is increased, the conformation on the right is favoured over the conformation on the left. The preference for more elongated chains results in alkyl chain-separated polar groups that move slightly closer to each other as the temperature is increased, in agreement with the experimental data. This speculative model is strongly supported by the distribution of angles formed by the linking alkyl chain in $n = 12$ DIL, shown in Fig. S6.† Chain conformations spanning the range from ~90° to ~160° are clearly visible at all three temperatures. However, a larger population of angles become widened with the increase of temperature, indicating the elongated chains at higher temperatures. At this point, it is difficult to decide whether the observed structural features might be common in a broader class of DILs. We hope that this study inspires more work to explore this interesting question.

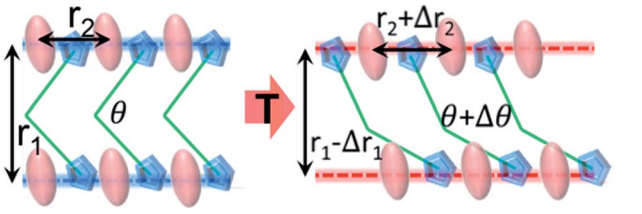

Fig. 6 The alkyl chain separated polar groups, separated by a distance r_1, in the $n = 12$ DIL adopt several configurations that span alkyl chain bending angles from ~90° to ~160°. As temperature increases, the alkyl chain bending angle within an increasing fraction of dications increases, r_1 decreases, and the close-contact distances between ions increase.

Ion pair/ion cage stability

The dynamical properties of dicationic $[C_n(mim)_2](Tf_2N)_2$ are less frequently reported in comparison to structural properties, but have great relevance for practical applications. Ishida *et al.* investigated the relaxation process of the DIL $[C_6(mim)_2](Tf_2N)_2$, and compared it to its monocationic analogue $[C_3mim][Tf_2N]$ using MD simulations,[32] in which they attributed the heterogeneous dynamics in DIL to its structural heterogeneity. Moreover, imidazolium-based DILs have been reported to exhibit higher stability than corresponding monocationic analogues,[33] which is related to slower translational motion or diffusion in DILs as demonstrated in the studies of both Ishida[32] and Yeganegi.[21]

In this section, the ion pair/ion cage time correlation functions of DILs will be studied with the goal of exploring the stabilities of ion pairs and diffusion-limiting cage-like structures at the nanoscale. An ion pair is defined as an anion with closest contact with the central cation and an ion cage is formed by all the anions in the first neighbouring shell of a central cation, which are determined by the radial distribution function of cation–anion. Zhao *et al.* have suggested that no long-lived ion pairs exist in ionic liquids, based on calculated correlated motion of cations and anions.[34]

Zhang *et al.* then correlated the high stability of ion pairs in RTILs with their thermophysical properties, *i.e.,* high melting points and high viscosities.[35] Both of these studies have concentrated on MILs, while the stability of ion pair/ion cage formations in DILs remained unexplored. Here, we calculate the ion pair/ion cage time correlation function $C(t)$ using the following equation:

$$C(t) = \frac{\langle h(0)h(t)\rangle}{\langle h\rangle}$$

where $h(t)$ is unity when a particular ion pair or ion cage is formed at time t, and zero otherwise. The calculated ion pair correlation functions for $[C_n(mim)_2](Tf_2N)$ and $[C_nmim][Tf_2N]$ at 320 K are shown in Fig. 7.

It can be seen that ion pair correlation functions for $[C_n(mim)_2](Tf_2N)_2$ decay slower than those of monocationic $[C_nmim][Tf_2N]$, indicating the higher stability of dication–anion pairs in DILs compared to MILs. The self-diffusion coefficients of dications are thus much smaller than those of their monocationic analogues (*e.g.* $[C_3(mim)_2]^{2+}$: 1.71 × 10^{-12} m^2 s^{-1}; $[C_3mim]^+$: 1.08 × 10^{-11} m^2 s^{-1}). Additionally, the ion pair

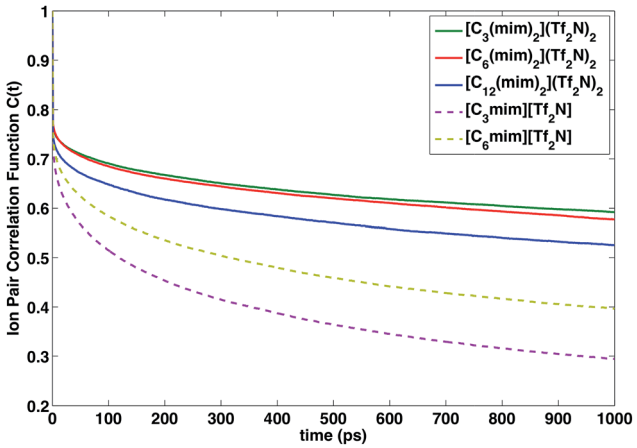

Fig. 7 Ion pair correlation functions of dicationic $[C_{12}(mim)_2](Tf_2N)_2$ (solid lines) and monocationic $[C_n mim][Tf_2N]$ (dashed lines) calculated from MD simulations at 320 K.

stability in DILs exhibits weaker chain-length dependence in comparison to MILs. With the increase of alkyl chain length in $[C_n(mim)_2](Tf_2N)_2$, a slight decrease in ion pair stability is noticed, accompanied by a higher diffusion coefficient, as was already reported in the study of Yeganegi *et al.*[21] However, the chain-length dependent ion pair stability is reversed in monocationic $[C_n mim][Tf_2N]$. Long-chain $[C_6mim][Tf_2N]$ shows higher ion pair stability than short-chain $[C_3mim][Tf_2N]$, which is related to the slower diffusion of long-chain $[C_6mim][Tf_2N]$, as evidenced by Broadband Dielectric Spectroscopy (BDS) and Pulsed Field Gradient Nuclear Magnetic Resonance (PFG-NMR) measurement.[36]

The ion-cage time correlation function (see Fig. 8) decays faster compared to the corresponding ion pair time correlation function, consistent with a previous study carried out on MILs.[35] Similar to ion pairs, the ion cages formed in DILs are more stable than those in MILs. However, a different chain-length dependence of the ion cage relaxation was observed. Long-chain

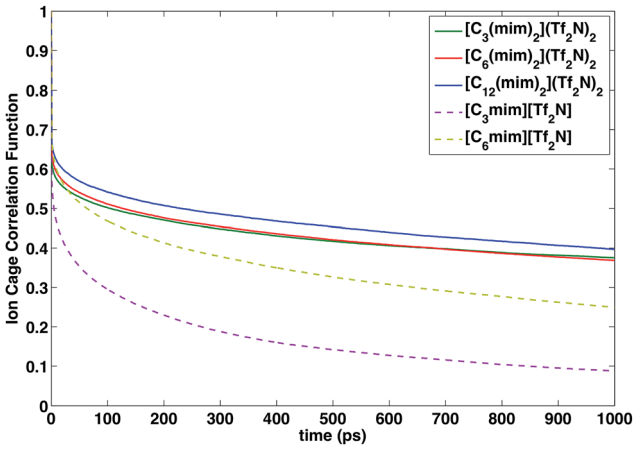

Fig. 8 Ion cage correlation functions of dicationic $[C_{12}(mim)_2](Tf_2N)_2$ (solid lines) and monocationic $[C_n mim][Tf_2N]$ (dashed lines) calculated from MD simulations at 320 K.

$[C_{12}(mim)_2](Tf_2N)_2$ exhibits the slowest decay, indicating the longest life time of ion cages. This finding is inconsistent with the chain length dependent increase of diffusion coefficients of anions in DILs ($[C_3(mim)_2](Tf_2N)_2$: 2.35×10^{-12} m^2 s^{-1} < $[C_6(mim)_2](Tf_2N)_2$: 2.71×10^{-12} m^2 s^{-1} < $[C_{12}(mim)_2](Tf_2N)_2$: 3.00×10^{-12} m^2 s^{-1}). However, according to the measurement of Shirota *et al.*,[33] the viscosity of $[C_n(mim)_2](Tf_2N)_2$ is not linearly dependent on the alkyl chain length, which decreases for short chains and then increases as the chain length increases. This trend is not captured by the molecular dynamics simulations in this work.

For MILs, short-chain $[C_3mim][Tf_2N]$ still exhibits a faster decay than $[C_6mim][Tf_2N]$, consistent with their ion pair correlation function. Compared to DIL $[C_n(mim)_2](Tf_2N)_2$, the differences of ion cage stability between monocationic $[C_3mim][Tf_2N]$ and $[C_6mim][Tf_2N]$ are more pronounced, likely caused by the big differences in the anion diffusion coefficients (*e.g.* $[C_6mim][Tf_2N]$: 9.55×10^{-12} m^2 s^{-1} *vs.* $[C_3mim][Tf_2N]$: 6.82×10^{-12} m^2 s^{-1}). In general, both the ion pairs and ion cages formed in DIL $[C_n(mim)_2](Tf_2N)_2$ exhibit a longer life time than in MIL $[C_n mim][Tf_2N]$. This is possibly due to the stronger Columbic network formed in DILs due to the additional positively charged cation head in dications.

Conclusions

This work explores the structural and dynamical properties in a series of typical DILs, $[C_n(mim)_2](Tf_2N)_2$ ($n = 3$, 6, and 12), using MD and SWAXS. Enhanced structural heterogeneity in $[C_n(mim)_2](Tf_2N)_2$ and elongation changes of the alkyl chain with temperature were studied for the first time by SWAXS and MD simulation. Moreover, it was found that temperature variation does not impose a significant influence on the structural assembly of nonpolar alkyl chains or polar cation heads and anions, which is evidenced by only negligible changes in the heterogeneity order parameters at different temperatures. In contrast to its MIL counterpart, $[C_6mim][Tf_2N]$, DIL $[C_{12}(mim)_2](Tf_2N)_2$ exhibits a prepeak at 0.4 Å^{-1} at all temperatures studied, indicating a non-obvious aggregation of linkage alkyl chains, consistent with a previous finding for DIL $[C_n(mim)_2](BF_4)_2$.[19] It was demonstrated that the different trends of temperature dependent prepeak shifts observed in $[C_n(mim)_2](Tf_2N)_2$ and other MILs correlate with the type of ionic liquids.

Additionally, the ion pair/ion cage stability, an indicator of the dynamical properties of RTILs, was investigated. It is found that in both DILs and MILs, the ion pair stability is consistent with the translational mobility of ions similar to previous studies.[35] MILs of the type $[C_n mim][Tf_2N]$ show a diffusion-dominating ion cage stability, whereas DILs show the opposite trend, suggesting more complicated dynamics in DILs, which are not captured by MD simulation. Therefore, an optimized force field with high accuracy is needed to study the dynamic properties of DILs $[C_n mim][Tf_2N]$ in greater detail. In addition, in the DILs $[C_n(mim)_2](Tf_2N)_2$, both ion pair and ion cage effects possess a longer life time than in MILs, probably resulting from the stronger Columbic network of divalent ions, which may be

the cause of the temperature insensitive structural variation in DILs as well.

Acknowledgements

This material is based upon work supported as part of the Fluid Interface Reactions, Structures and Transport (FIRST) Center, an Energy Frontier Research Center funded by the U.S. Department of Energy, Office of Science, Office of Basic Energy Sciences. The X-ray scattering portion of this research was conducted at the Center for Nanophase Materials Sciences, which is sponsored at Oak Ridge National Laboratory by the Scientific User Facilities Division, Office of Basic Energy Sciences, U.S. Department of Energy. We also would like to thank the National Energy Research Scientific Computing Center (NERSC) for providing computational resources, which is supported by the Office of Science of the U.S. Department of Energy under Contract no. DE-AC02-05CH11231.

References

1 Y. Wang and G. A. Voth, *J. Am. Chem. Soc.*, 2005, **127**, 12192–12193.
2 Y. Wang and G. A. Voth, *J. Phys. Chem. B*, 2006, **110**, 18601–18608.
3 H. V. R. Annapureddy, H. K. Kashyap, P. M. Biase and C. J. Margulis, *J. Phys. Chem. B*, 2010, **114**, 16838–16846.
4 A. Triolo, O. Russina, B. Fazio, R. Triolo and E. Di Cola, *Chem. Phys. Lett.*, 2008, **457**, 362–365.
5 C. S. Santos, N. S. Murthy, G. A. Baker and E. W. Castner, *J. Chem. Phys.*, 2011, **134**, 121101.
6 C. S. Santos, H. V. R. Annapureddy, N. S. Murthy, H. K. Kashyap, E. W. Castner and C. J. Margulis, *J. Chem. Phys.*, 2011, **134**, 064501.
7 A. Triolo, O. Russina, H. J. Bleif and E. Di Cola, *J. Phys. Chem. B*, 2007, **111**, 4641–4644.
8 B. L. Bhargava, R. Devane, M. L. Klein and S. Balasubramanian, *Soft Matter*, 2007, **3**, 1395–1400.
9 J. J. Hettige, H. K. Kashyap, H. V. R. Annapureddy and C. J. Margulis, *J. Phys. Chem. Lett.*, 2013, **4**, 105–110.
10 H. K. Kashyap, J. J. Hettige, H. V. R. Annapureddy and C. J. Margulis, *Chem. Commun.*, 2012, **48**, 5103–5105.
11 H. K. Kashyap, C. S. Santos, H. V. R. Annapureddy, N. S. Murthy, C. J. Margulis and E. W. Castner, *Faraday Discuss.*, 2012, **154**, 133–143.
12 A. A. H. Padua and J. N. A. C. Lopes, *J. Phys. Chem. B*, 2006, **110**, 3330–3335.
13 S. Li, J. L. Banuelos, J. Guo, L. Anovitz, G. Rother, R. W. Shaw, P. C. Hillesheim, S. Dai, G. A. Baker and P. T. Cummings, *J. Phys. Chem. Lett.*, 2012, **3**, 125–130.
14 X. X. Han and D. W. Armstrong, *Org. Lett.*, 2005, **7**, 4205–4208.
15 D. Fang, J. M. Yang and C. M. Jiao, *ACS Catal.*, 2011, **1**, 42–47.
16 F. Pagano, C. Gabler, P. Zare, M. Mahrova, N. Dorr, R. Bayon, X. Fernandez, W. H. Binder, M. Hernaiz, E. Tojo and A. Igartua, *Proc. Inst. Mech. Eng., Part J*, 2012, **226**, 952–964.
17 W. J. Cho, C. G. Yeom, B. C. Kim, K. M. Kim, J. M. Ko and K. H. Yu, *Electrochim. Acta*, 2013, **89**, 807–813.
18 S. Li, K. L. Van Aken, J. K. McDonough, G. Feng, Y. Gogotsi and P. T. Cummings, *J. Phys. Chem. C*, 2014, **118**, 3901–3909.
19 S. Li, G. Feng, J. L. Banuelos, G. Rother, P. F. Fulvio, S. Dai and P. T. Cummings, *J. Phys. Chem. C*, 2013, **117**, 18251–18257.
20 X. Qiu, J. W. Thompson and S. J. L. Billinge, *J. Appl. Crystallogr.*, 2004, **37**, 678.
21 S. Yeganegi, A. Soltanabadi and D. Farmanzadeh, *J. Phys. Chem. B*, 2012, **116**, 11517–11526.
22 J. L. Anderson, R. F. Ding, A. Ellern and D. W. Armstrong, *J. Am. Chem. Soc.*, 2005, **127**, 593–604.
23 J. N. C. Lopes, J. Deschamps and A. A. H. Padua, *J. Phys. Chem. B*, 2004, **108**, 2038–2047.
24 B. Hess, H. Bekker, H. J. C. Berendsen and J. G. E. M. Fraaije, *J. Comput. Chem.*, 1997, **18**, 1463–1472.
25 U. Essmann, L. Perera, M. L. Berkowitz, T. Darden, H. Lee and L. G. Pedersen, *J. Chem. Phys.*, 1995, **103**, 8577–8593.
26 H. J. C. Berendsen, D. Vanderspoel and R. Vandrunen, *Comput. Phys. Commun.*, 1995, **91**, 43–56.
27 O. Borodin, W. Gorecki, G. D. Smith and M. Armand, *J. Phys. Chem. B*, 2010, **114**, 6786–6798.
28 Y. M. Ji, R. Shi, Y. T. Wang and G. Saielli, *J. Phys. Chem. B*, 2013, **117**, 1104–1109.
29 K. Shimizu, C. E. S. Bernardes and J. N. C. Lopes, *J. Phys. Chem. B*, 2014, **118**, 567–576.
30 C. E. S. Bernardes, K. Shimizu, A. I. M. C. L. Ferreira, L. M. N. B. F. Santos and J. N. C. Lopes, *J. Phys. Chem. B*, 2014, **118**, 6885–6895.
31 E. Bodo, M. Chiricotto and R. Caminiti, *J. Phys. Chem. B*, 2011, **115**, 14341–14347.
32 T. Ishida and H. Shirota, *J. Phys. Chem. B*, 2013, **117**, 1136–1150.
33 H. Shirota, T. Mandai, H. Fukazawa and T. Kato, *J. Chem. Eng. Data*, 2011, **56**, 2453–2459.
34 W. Zhao, F. Leroy, B. Heggen, S. Zahn, B. Kirchner, S. Balasubramanian and F. MuÃàller-Plathe, *J. Am. Chem. Soc.*, 2009, **131**, 15825–15833.
35 Y. Zhang and E. J. Maginn, *Phys. Chem. Chem. Phys.*, 2012, **14**, 12157–12164.
36 J. R. Sangoro, C. Iacob, S. Naumov, R. Valiullin, H. Rexhausen, J. Hunger, R. Buchner, V. Strehmel, J. Karger and F. Kremer, *Soft Matter*, 2011, **7**, 1678–1681.

